PAPER *Special Section on Discrete Mathematics and Its Applications*

Digital Curve Approximation with Length Evaluation

Tetsuo ASANO[†a)], ***Regular Member***, **Yasuyuki KAWAMURA**[†], ***Student Member***, **Reinhard KLETTE**[††], ***Nonmember***, ***and*** **Koji OBOKATA**[†], ***Regular Member***

SUMMARY The purpose of this paper is to discuss length estimation based on digitized curves. Information on a curve in the Euclidean plane is lost after digitization. Higher resolution supports a convergence of a digital image towards the original curve with respect to Hausdorff metric. No matter how high resolution is assumed, it is impossible to know the length of an original curve exactly. In image analysis we estimate the length of a curve in the Euclidean plane based on an approximation. An approximate polygon converges to the original curve with an increase of resolution. Several approximation methods have been proposed so far. This paper proposes a new approximation method which generates polygonal curves closer (in the sense of Hausdorff metric) in general to its original curves than any of the previously known methods and discusses its relevance for length estimation by proving a Convergence Theorem.

key words: *approximating sausage, digital curve, digital geometry, length of a curve, multigrid convergence, perimeter*

1. Introduction

Recent progress in the technology of high-quality image representations supports finer grid resolutions, which allow visually improved and more accurate images of digitized curves. However, increase in grid resolution is insufficient to keep all information available in the original continuous image. This is caused by an information loss due to digitization from a continuous space into a discrete space. For example, the length of a curve may change considerably by digitization. First of all, it is not easy to define the length of a curve in a digital image or to measure the 'correct' length of a digitized curve. As we increase the resolution of an image, a digitized curve looks visually closer to the original continuous one (reflecting convergence with respect to the Hausdorff metric. Hausdorff metric measures the degree of mismatch of two polygons). However, this does not imply that the length of a digitized curve converges to that of the original curve [5]. Figure 1 shows that the length of the staircase remains constant and is not converging towards the length of an original diagonal line, no matter how large the grid resolution is chosen.

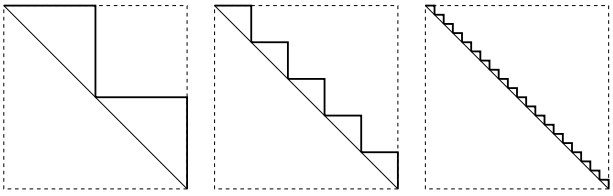

Fig. 1 The staircase curve is a good approximation of the diagonal line with respect to a Hausdorff metric. However, the length of the staircase line remains constant.

The digital approximation of a planar curve is one of the important topics in image analysis. An approximation scheme is required to ensure convergence of estimated properties such as diameter, moments, or curve length towards true values (of the curve before digitization) as the grid resolution increases. For example, the *digital straight segment approximation method* (DSS method, in short), see [3], [8], and the *minimum length polygon approximation method* assuming one-dimensional grid continua as boundary sequences (GC-MLP method), see [9], are methods for which there are convergence theorems when specific convex sets are assumed to be given input data, see [5], [7], [10]. This paper studies the convergence property of a new minimum length polygon approximation method based on so-called *approximating sausages*. Here after, our method is refered to as AS-MLP method.

Motivations for studying this new technique are as follows: the resulting DSS approximating polygon depends upon starting point and the orientation of the boundary scan, it is not uniquely defined, but it may be calculated for any given digital object. The resulting GC-MLP approximation polygon is uniquely defined, but it assumes a one-dimensional grid continua as an input polygon which is only possible if a given digital object does not have cavities of width 1 or 2. The new method generates a uniquely defined polygon, and it can be computed for any given digital object.

Another advantage of our new method becomes clear by studying resulting shapes. The approximated curves obtained by the previous methods DSS and GC-MLP have a Hausdorff distance at least (DSS), or exactly (GC-MLP) equal to the grid constant from the original curves. In a number of experiments we could

Manuscript received August 20, 2002.
Manuscript revised November 4, 2002.
Final manuscript received December 29, 2002.

[†]The authors are with the School of Information Science, Japan Advanced Institute of Science and Technology, Ishikawa-ken, 923-1292 Japan.
[††]The author is with the CITR, University of Auckland, Tamaki Campus, Building 731, Auckland, New Zealand.
a) E-mail: t-asano@jaist.ac.jp

statistically verify that approximated curves created by DSS often have 'sharp angles' and those by GC-MLP may be 'shifted away' from the original curve location. Our new approximation scheme AS-MLP generates 'better fitted' shapes in many cases.

In this paper first we provide some preliminary definitions and propose our new approximation method AS-MLP. Then, we prove a convergence theorem. Finally we compare this method with other methods by discussing experimental results.

2. Preliminaries and Previous Works

Let r be the grid resolution defined as being the number of grid points per unit length. We consider *r-grid points* $g^r_{i,j} = (i/r, j/r)$ in the Euclidean plane, for integers i, j. Any r-grid point is assumed to be the center point of an *r-square* with *r-edges* of length $1/r$ parallel to the coordinate axes, and *r-vertices*.

Let S be a simply-connected compact set in the Euclidean plane, called *real preimage*. The frontier of S defines the simple curve of interest. The set $C_r(S)$ is the union of all those r-squares whose center points g^r_{ij} are in S. We call this boundary $\partial C_r(S)$ the *r-frontier* of S. The frontier $\partial C_r(S)$ may consist of several non-connected curves even in the case of a convex set S. A set S is *r-compact* iff there is a number $r_0 > 0$ such that $\partial C_r(S)$ is just one (connected) curve for any $r \geqq r_0$. This definition of r-compactness has been introduced in [6] in the context of showing multigrid convergence of the DSS method.

Given a connected region S in the Euclidean plane and a grid resolution r, the r-frontier of S is uniquely determined. We consider r-compact sets S, and grid resolutions $r \geqq r_0$ for such a set, i.e. $\partial C_r(S)$, the frontier of $C_r(S)$, is just one (connected) curve.

DSS scheme: DSS segmentation algorithm traces an r-frontier, i.e., an alternating sequence of r-vertices and r-edges, and subdivides it into maximum length digital straight segments. This algorithm detects for each maximum length DSS(Digital Straight line Segment), the coordinates of its end points (two r-vertices) and calculates the length of each DSS as the Euclidean distance between these two points. The sum of the lengths of these DSS's is finally used as DSS estimator of the perimeter.

Let S be a bounded subset of the Euclidean plane, $I_r(S)$ be the union of all closed r-squares completely contained in the interior of S, and $O_r(S)$ be the union of all r-squares having a non-empty intersection with set S. The open set $O_r(S) \setminus (I_r(S) \cup \partial O_r(S))$ is an *open r-boundary* of set S.

An open r-boundary is finite, alternating sequence of r-edges and r-squares if the set S is bounded. Open r-boundaries consist of a finite number of r-squares and r-edges. Any run around an open r-boundary passes through an alternating sequence of r-squares and r-edges.

GC-MLP scheme: GC-MLP algorithm makes the shortest polygonal Jordan curve, which encircles $I_r(S)$, in the open r-boundary of S. The length of this curve is used as GC-MLP estimator of the perimeter.

3. New Approximation Scheme AS-MLP

The digitization model for our new approximation method is just the same as that considered in case of the DSS method, that is, the r-frontier of S. In such a case the r-frontier of S can be represented in the form $P = (v_0, v_1, \ldots, v_{n-1})$ in which the vertices are clockwise ordered so that the interior of S lies to the right of the boundary. Note that all arithmetics on vertex indices is modulo n.

Let δ be a real number between 0 and $1/2r$. For each vertex of P we define forward and backward shifts: A *forward shift* $f(v_i)$ of v_i is a point on the edge (v_i, v_{i+1}) at the distance δ from v_i. A *backward shift* $b(v_i)$ is that on the edge (v_{i-1}, v_i) at the distance δ from v_i.

For example, in the approximation scheme described below we will replace an edge (v_i, v_{i+1}) by a line segment $(v_i, f(v_{i+1}))$ interconnecting v_i and the forward shift of v_{i+1}, which is referred to as the *forward approximating segment* and denoted by $L_f(v_i)$. The *backward approximating segment* $(v_i, b(v_{i-1}))$ is defined similarly and denoted by $L_b(v_i)$. Refer to Fig. 2 for illustration. Now we have three sets of edges, original edges of the r-frontier, forward and backward approximating segments. Based on these edges we define a connected region $A_r(S)$, which is homeomorphic to the annulus, as follows:

Given a polygonal circuit P describing an r-frontier in clockwise orientation, by reversing P we obtain a polygonal circuit Q in the counterclockwise order. In the initialization step of our approximation procedure we consider P and Q as the *external* and *internal* bounding polygons of a polygon P_B homeomorphic to the annulus. It follows that the area of this initial polygon P_B zero, and as a set of points it coincides with $\partial C_r(S)$. In the next step, we add all forward and backward approximating segments to P or Q in order to increase the area of the polygon P_B. For any forward or backward approximating segment $L_f(v_i)$ or $L_b(v_i)$, we first remove the part lying in the interior of the current polygon P_B and updating the polygon P_B

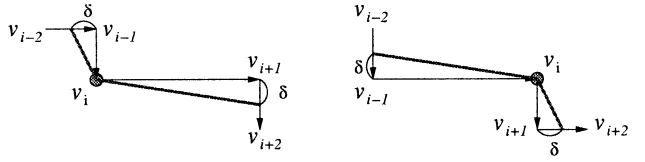

Fig. 2 Definition of the forward and backward approximating segments associated with a vertex v_i.

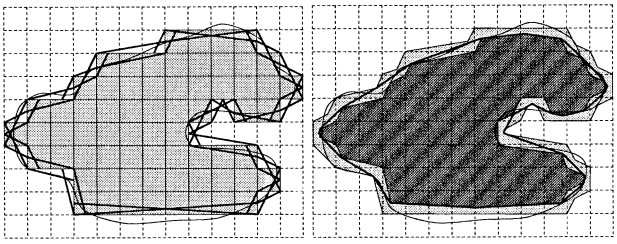

Fig. 3 Construction of approximating sausage and approximation by shortest internal path.

by adding the remaining part of the segment as a new boundary edge. The direction of the edge is determined so that the interior of P_B lies to its right. The resulting polygon P_B contains $\partial C_r(S)$, and where the Hausdorff distance between P and Q becomes non-zero, i.e., the internal and external boundaries of P_B do not touch each others.

Definition 3.1: The resulting polygon P_B is referred to as the *approximating sausage* of the r-frontier of S and denoted by $A_r(S)$.

The width of such an approximating sausage depends on the value of δ. It is easy to see that as far as the value of δ is at most half of the grid size, i.e., less than or equal to $1/2r$, the approximating sausage $A_r(S)$ is well defined, that is, it has no self-intersection. It is also immediately clear from the definition that the Hausdorff distance from the r-frontier $\partial C_r(S)$ to the boundary of the sausage $A_r(S)$ is at most $\delta \leqq 1/2r$. In this paper, we implicitly assume $\delta = 1/2r$.

We are ready to define the final step in our AS-MLP approximation scheme for estimating the length of a digital curve. Our method is similar to that of the GC-MLP introduced in [9].

Definition 3.2: Assume a region S having a connected r-frontier. An *AS-MLP curve* for approximating the boundary of S is defined as being a shortest closed curve $\gamma_r(S)$ lying entirely in the interior of the approximating sausage $A_r(S)$, and encircling the internal boundary of $A_r(S)$.

It follows that such an AS-MLP curve $\gamma_r(S)$ is uniquely defined, and that it is a polygonal curve defined by finitely many straight segments. Note that this curve depends upon the choice of the approximation constant δ. An example of such a shortest closed curve $\gamma_r(S)$ is given in Fig. 3.

4. Properties of Digital Curves

We discuss some of the properties of the approximating polygonal curve $\gamma_r(S)$ defined above, assuming that $\partial C_r(S)$ is a single connected curve.

Non-selfintersection: The AS-MLP curve $\gamma_r(S)$ is defined to be a shortest closed curve lying in the approximating sausage. Since it is obvious from the definition that the sausage has no self-intersection, the curve has no self-intersection.

Controllability: The width of an approximating sausage can be controlled by selecting a value of δ.

Linear complexity: Due to the definition of our curve $\gamma_r(S)$ the number of its vertices is at most twice the number of vertices of the r-frontier.

Computational complexity: Assuming that a triangulation of an approximating sausage is given, linear computation time suffices to find a shortest closed path within the sausage: we can triangulate an approximating sausage in linear time since the vertices of the sausage can be calculated only using nearby segments. So, linear time is enough to triangulate it. Then, we can construct an adjacency graph, which is a tree, representing adjacency of triangles again in linear time. Finally, we can find a shortest path in linear time by slightly modifying the linear-time algorithm for finding a shortest path within a simple polygon.

5. Convergence Theorem

In this section we first prove the main result of this paper about the multigrid convergence of the AS-MLP curve based on the length estimation of the perimeter of a given set S. The multigrid convergences of the DSS and GC-MLP curves have been shown in [6].

Theorem 5.1: The length of the approximating polygonal curve $\gamma_r(S)$ converges to the perimeter of a given region S if S is an r-compact polygonal convex bounded set.

We begin a proof of this theorem by an investigation of some geometric properties of the r-frontier of a convex polygonal region S and then provide a series of lemmas so as to obtain Theorem 5.1.

We first classify r-grid points into interior and exterior points depending on whether they are located inside of the region S or not. Then, CH_{in} is defined to be the convex hull of the set of all interior r-grid points. That is, CH_{in} is the minimum convex polygon including all interior points. CH_{out} is defined to be the convex hull of the set which is obtained by 'expansion' of the set of interior r-grid points. Here, by expansion of a point set we mean including for each r-grid point its four neighbors into the point set. See Fig. 4 for illustration.

Lemma 5.2: Given an r-compact polygonal convex bounded set S, the approximating polygonal curve $\gamma_r(S)$ is contained in the region bounded by CH_{in} and CH_{out}.

Proof The P_B is contained in the region bounded by CH_{in} and CH_{out}. □

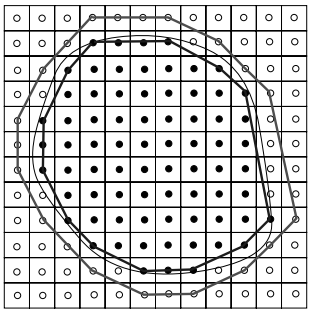

Fig. 4 Interior r-grid points (filled circles) and exterior points (empty circles) with CH_{in} and CH_{out}.

Lemma 5.3: The perimeter of CH_{out} is larger by $4\sqrt{2}/r$ than that of CH_{in}.

Proof The r-grid points which are added by expansion from r-grid points make CH_{out}. We classify edges of CH_{in} into four groups by their slopes θ: (i) $315° < \theta \leqq 45°$, (ii) $45° < \theta \leqq 135°$, (iii) $135° < \theta \leqq 225°$, and (iv) $225° < \theta \leqq 315°$. An r-grid point (i, j) on the convex hull CH_{in} produces a new r-grid point $(i+1, j)$, $(i, j+1)$, $(i-1, j)$, or $(i, j-1)$ if it is an endpoint of an edge of the first, second, third, and forth group, respectivly. All other intermediate r-grid points along those hull edges have the same property. Thus, an edge of CH_{in} in the first group ($315° < \theta \leqq 45°$) slides vertically down as an edge of CH_{out} and an edge in the second group ($45° < \theta \leqq 135°$) slides horizontally to the right, and so on. Since the r-grid point incident to two edges of different groups slides vertically and horizontally, the length of its associated edge is longer than that of the original one by $\sqrt{2}/r$. There are four such boundary points in total. Thus, we obtain the lemma. □

This lemma implies that the difference between the lengths of the two boundaries in an approximating sausage is exactly $4\sqrt{2}/r$ if both of them are convex. Now, we can prove the following lemma which will be of crucial importance for proving the convergence theorem.

Next, we discuss a worst-case bound for perimeter estimates by AS-MLP. We represent below the r-frontier as an alternating sequence of horizontal and vertical edges by merging any two consecutive r-edges having the same orientation, instead of an alternating sequence of unit r-edges and r-vertices. Edges consisting of more than one r-edge are called *long* edges. Due to the convexity of the region S, any such sequence must have the following four edges: (1) North horizontal edge e_N of the largest y-coordinate, (2) East vertical edge e_E of the largest x-coordinate, (3) South horizontal edge e_S of the smallest y-coordinate, and (4) West vertical edge e_W of the smallest x-coordinate.

Let e_N^{end} be the last long horizontal edge on the r-frontier we encounter before e_E when we follow it from the North edge e_N in clockwise order. If there is no such long edge, e_N^{end} is e_N itself. Similarly, let e_N^{start} be the last long horizontal edge on the r-frontier we encounter before e_N when we follow it from e_W in clockwise order. If there is no such long edge, e_N^{start} is e_N. Then, the North part of the r-frontier is defined as the part of it from e_N^{start} to e_N^{end}. The East, South, and West parts are similarly defined.

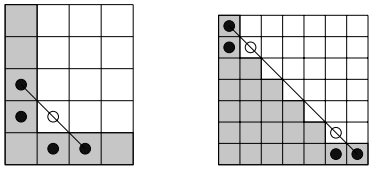

Fig. 5 A contradiction to the convexity of S.

The following lemma is obtained from the convexity of region in digital image.

Lemma 5.4: The North part of the r-frontier is well defined and includes no long vertical edge if an original set is convex.

Proof First of all, we observe that any long edge must be followed by a unit edge when the edge turns left. If there is a long edge following another long edge, the exterior point between the edges is in the region S because S is convex. This is a contradiction. If there is a long vertical edge between e_N and e_N^{end}, an exterior point causes similar contradiction. See Fig. 5. □

An approximating curve γ_r is not always convex though S is convex. Fortunately, we can prove that the concave part appears at most constant times.

Lemma 5.5: Given a convex region S in the continuous plane, the closed curve $\gamma_r(S)$, the approximation of its boundary by AS-MLP contains at most 8 concave parts.

Proof It is shown here that there is at most one concave part between e_N and e_N^{end}. It is easy to prove similar properties at the other 7 parts.

We set the origin as shown in Fig. 6 (below) and investigate p and q such that $\gamma_r(S)$ makes a concave part. The coordinates of the three points $P1$, $P2$, and $P3$ associated with a concave part of $\gamma_r(S)$ are given by $P1(\frac{-p}{4rp-r}, \frac{2p}{4rp-r}), P2(\frac{q}{4rq-r}, \frac{2q-1}{4rq-r}), P3(\frac{4q^2-2q}{4rq-r}, \frac{-2q+1}{4rq-r})$, respectively.

The condition for $P2$ lying below $P1P3$ can be expressed as follows:

$$P1P2 \times P1P3 > 0 \Leftrightarrow 2q^2 - (6p+1)q + 2p > 0.$$

Here, since p and q are natural numbers, $P2$ lies below $P1P3$ if $q > 3p$.

This condition may be satisfied only at the corner next to e_N. At the other corners, q depends on p as shown in Fig. 7. That is, $q \leqq p+1$ in such occasion, so a concave part does not appear. □

Due to the concave parts the length of the curve

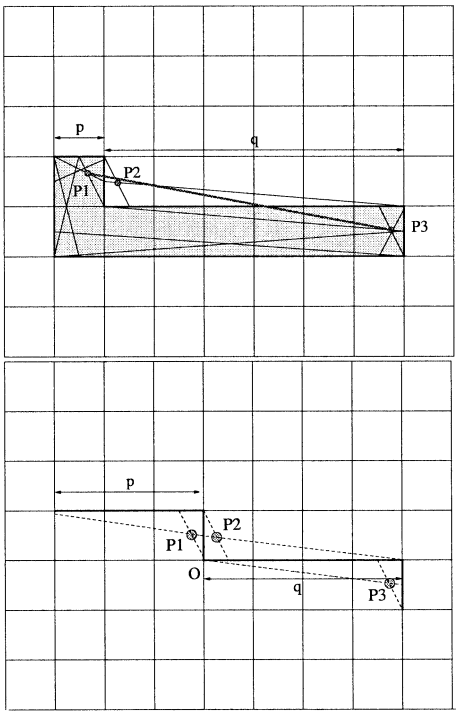

Fig. 6 Appearance of a concave part. (the size of pixel is $\frac{1}{r} \times \frac{1}{r}$)

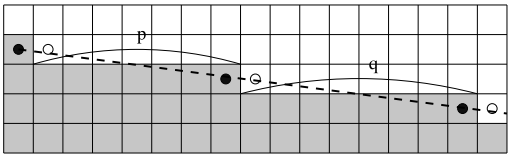

Fig. 7 Dependency of q on p. q cannot be longer than $p+1$. Since a long edge appears after a vertical unit edge, inner points (black) must lie below the line and outer points (white) must lie above the line.

$\gamma_r(S)$ can be longer than that of the convex hull of $\gamma_r(S)$. We will argue how large the difference can be for each concave part.

Lemma 5.6: The approximating curve $\gamma_r(S)$ is longer by at most $0.02334/r$ than the convex hull of $\gamma_r(S)$ at an concave part.

Proof Here is a sketch of the proof. See Appendix for details. When the coordinates of three points $P1, P2$ and $P3$ are defined as before, the difference of $\gamma_r(S)$ and the perimeter of its convex hull can be computed as $d = P1P2 + P2P3 - P1P3$.

d is a function in p and q, which is monotonically decreasing in p for any q. Since p and q are natural numbers, we can see $d < 0.02334/r$. □

Combining the observations above, we have the theorem required.

Lemma 5.7: When S is a finite convex region in the Euclidean space, there is r_0 such that the following condition is satisfied for all $r > r_0$: the approximating curve $\gamma_r(S)$ obtained by AS-MLP from $C_r(S)$ forms a simple polygon and its length l_r satisfies

$$|Perimeter(S) - l_r| \leqq (4\sqrt{2} + 8 \times 0.0234)/r \approx 5.84/r$$

where $Perimeter(S)$ denotes the perimeter of S.

This theorem guarantees the convergence of the perimeter of a convex region to its true length with increasing resolution.

6. Visual Comparisons for Non-Convex Regions

The previous theorem shows that AS-MLP can approximate a convex region with a guaranteed upper error bound for length estimates. However an effective approximation for general non-convex regions is expected and AS-MLP can be applied to such regions. This section gives actual comparisons of approximations scheme for such general regions.

Figure 8 gives visual comparisons of the proposed method with the existing schemes.

Here is an example to show superiority of AS-MLP over DSS and GC-MLP. Consider a comb shape shown in Fig. 9. Figure 10 illustrates the results produced by DSS and GC-MLP where concave parts are extremely narrow. It is seen that DSS makes notches and GC-MLP fills concave parts, so these schemes are not appropriate for such an image. However, AS-MLP does not fill concavities. A standard AS-MLP with $\delta = 0.5$ generates an approximating curve similar to that obtained by DSS. An approximating curve by AS-MLP becomes close to the simple boundary of the set of pixels $C_r(S)$ for a smaller value of δ. On the other hand, for a larger value of δ, an angular shape disappears. In short, AS-MLP can control results by varying δ.

Figure 11 shows the result of approximations for comb shape region, which looks like the same set as the one in Fig. 9, for a four times finer resolution. Because of high resolution, GC-MLP can also approximate without filling concave parts and DSS is the same as r-frontier $C_r(S)$. It is seen in Fig. 11 that AS-MLP can control roundish apophysis. Thus, for a high resolution image, standard AS-MLP approximates like GC-MLP and for $\delta = 0$, it does as DSS.

It may be understood in an example of "comb" that, for high resolution image, every approximation scheme makes a curve close to the r-frontier $\partial C_r(S)$ and they are quite similar to each other. For a low resolution image, a complicated region is approximated to that is quite different from the preimage. Figure 12 is one of examples in which the convexities are so small to approximate and convex and concave parts altanately appear. It is well observed in Fig. 13 that AS-MLP approximates more naturally than DSS and GC-MLP.

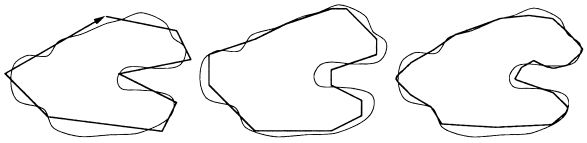

Fig. 8 Different approximated curves created by the three methods: DSS (left), GC-MLP (center), and AS-MLP (right).

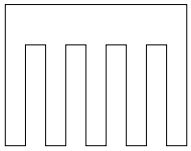

Fig. 9 Comb shape. (the width of a concaved part is $1/r$)

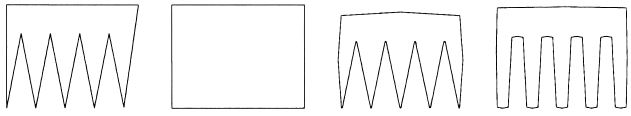

Fig. 10 Approximating curves for Fig. 9. To the order from the left DSS, GC-MLP, standard AS-MLP ($\delta = 0.5$) and AS-MLP with $\delta = 0.2$.

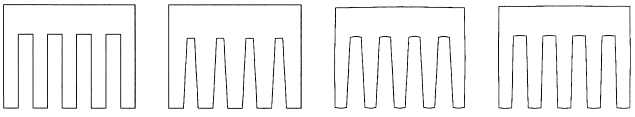

Fig. 11 Approximating curves for a comb shaped region (the same as Fig. 9) with fine resolution. From left to right: DSS, GC-MLP, standard AS-MLP with $\delta = 0.5$ and AS-MLP with $\delta = 0.2$.

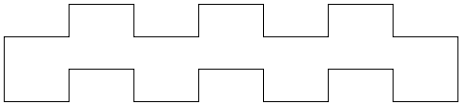

Fig. 12 A region which has many small convex and concaved parts.

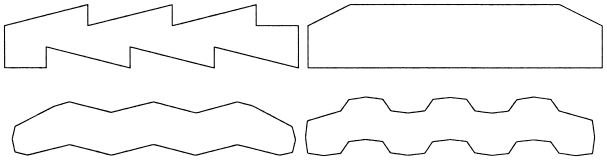

Fig. 13 Approximations of the object in Fig. 12. The results shown above are ones by the previous schemes (left: DSS, right: GC-MLP) and below are ones by AS-MLP. (left: $\delta = 0.5$, right:$\delta = 0.25$)

7. Experimental Evaluation

We have seen above that the error by AS-MLP is bounded in theory by $5.8/r$ for a grid resolution r for convex polygons. To see its practical behavior we have done experiments on various curves, which are described below. Although we have restricted ourselves to convex objects in a convergence theorem, we took non-convex curves as well. Figure 14 illustrates a set of objects used for experiments.

Fig. 14 Experimental objects.

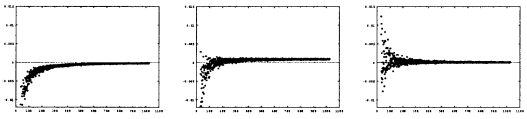

(a) estimation error for CIRCLE

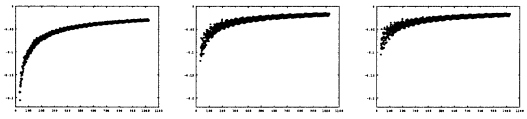

(b) estimation error for COMMA

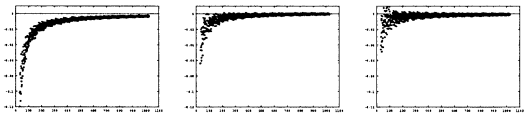

(c) estimation error for CRESCENT

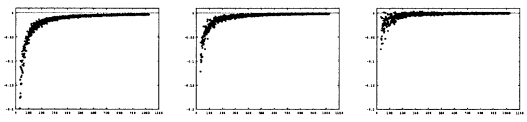

(d) estimation error for SINC

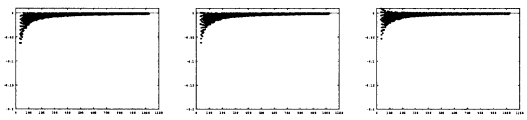

(e) estimation error for SQUARE

Fig. 15 Experimental results. The performances of GC-MLP, AS-MLP and DSS are arranged from left to right in each row in the figures.

CIRCLE: the equation of the circle is $(x-0.5)^2 + (y-0.5)^2 = 0.4^2$.

COMMA: the shape of "comma" is composed of three circular arcs. The lower arc is a part of CIRCLE. The upper arcs are circular arcs whose radii are half of CIRCLE.

CRESCENT: the crescent object is the remainder of two circles with the two centers separated by 0.28.

SINC: the equation of "sinc" corresponding to the upper curve is $y = \frac{\sin(16\pi x)}{64\pi x}$. Other edges are parts of SQUARE.

SQUARE: each edge of SQUARE is parallel to axis and its length is 0.8.

We have implemented the three approximating schemes, DSS, GC-MLP, and our AS-MLP for comparisons (DSS and GC-MLP based on source code provided by the authors of [4]). We have computed the approximating curve lengths against the true perimeter of a given set S. The error E_{DSS} of DSS approximating scheme is defined by

$$E_{DSS} = \frac{P(S) - P(DSS_S)}{P(S)}$$

where $P(S)$ is the true perimeter of S and $P(DSS_S)$ is the perimeter of the approximation polygon by DSS scheme. E_{MLP} and E_{ASMLP} are similarly defined.

Figures 15(a)–(e) show the errors for the listed objects used in the experiments. The performances of GC-MLP, AS-MLP and DSS are arranged from left to right in each row in the figures. It may be clear from these graphs that AS-MLP has higher performance than GC-MLP does, but DSS is the best among the three.

8. Conclusion

This paper proposes the AS-MLP scheme for a finite convex region and compares it with the previous schemes of DSS and GC-MLP. The properties of the AS-MLP scheme are: (1) more natural approximation is obtained than by the previous schemes, (2) it is more accurate than GC-MLP and (3) the resulting curve is uniquely determined while DSS may produce differnt curves depending on starting points and orientation. The greatest advantage of AS-MLP is the controllability of resulting shapes for lower resolution by parameter variation.

References

[1] T. Asano, Y. Kawamura, R. Klette, and K. Obokata, "A new approximation scheme for digital objects and curve length estimations," Proc. Image and Vision Computing New Zealand, pp.26–31, Hamilton, Nov. 2000.

[2] T. Buelow and R. Klette, "Rubber band algorithm for estimating the length of digitized space-curves," Proc. ICPR'00, vol.III, pp.551–555, IEEE, Barcelona, Sept. 2000.

[3] A. Hübler, R. Klette, and K. Voss, "Determination of the convex hull of a finite set of planar points within linear time," EIK (Elektron. Informationsverarbeitung und Kybernetik), vol.17, pp.121–139, 1981.

[4] R. Klette, V. Kovalevsky, and B. Yip, "On the length estimation of digital curves," Proc. Vision Geometry VIII, SPIE, vol.3811, pp.117–129, Denver, July 1999.

[5] R. Klette and B. Yip, "The length of digital curves," Machine GRAPHICS & VISION 9, pp.673–703, 2000.

[6] R. Klette and J. Zunic, "Multigrid convergence of calculated features in image analysis," J. Mathematical Imaging and Vision 13, pp.173–191, 2000.

[7] V. Kovalevsky, and S. Fuchs, "Theoretical and experimental analysis of the accuracy of perimeter estimates," in Robust Computer Vision, ed. W. Förstner and S. Ruwiedel, Wichmann, Karlsruhe, pp.218–242, 1992.

[8] A. Rosenfeld, "Digital straight line segments," IEEE Trans. Comput., vol.C-23, no.12, pp.1264–1269, 1974.

[9] F. Sloboda, B. Zaťko, and P. Ferianc, "Minimum perimeter polygon and its application," in Theoretical Foundations of Computer Vision, ed. R. Klette and W.G. Kropatsch, Mathematical Research 69, pp.59–70, Akademie Verlag, Berlin 1992.

[10] F. Sloboda, B. Zaťko, and J. Stoer, "On approximation of planar one-dimensional continua," in Advances in Digital and Computational Geometry, ed. R. Klette, A. Rosenfeld, and F. Sloboda, pp.113–160, Springer, Singapore, 1998.

Appendix: Proof of Lemma 5.6

Proof First, it is shown that $d = d(p,q)$ decreases monotonically in p for any q. For three points $P1, P2, P3$ determining a concave part, we rotate $P3$, $P1, P2$ to make $P2P3$ horizontal and let $P2$ coincide with the origin in new coordinates. Let these three points be mapped from $P1, P2, P3$ into $S(x,y), O, T(l,0)$, respectively, and the line which S moves on by increasing p be $y = ax + b$. Figure A·1 illustrates this procedure. Note that $x = x(p)$ satisfies $\frac{d}{dp}x > 0$.

$$\begin{aligned} d &= P1P2 + P2P3 - P1P3 = SO + l - ST \\ &= \sqrt{x^2+y^2} + l - \sqrt{(x-l)^2+y^2} \\ &= \sqrt{x^2+(ax+b)^2} + l - \sqrt{(x-l)^2+(ax+b)^2} \end{aligned}$$

Since

$$\frac{d}{dx}\sqrt{x^2+(ax+b)^2} \leqq \frac{d}{dx}\sqrt{(x-l)^2+(ax+b)^2},$$

d reduces monotonically about p, Thus d is maximum at $p = 1$.

Here, we recall

$$\begin{aligned} d(p,q) &= P1P2 + P2P3 - P1P3 \\ &= \sqrt{\left(\frac{q}{r(4q-1)} + \frac{p}{r(4p-1)}\right)^2 + \left(\frac{2q-1}{r(4q-1)} - \frac{2p}{r(4p-1)}\right)^2} \end{aligned}$$

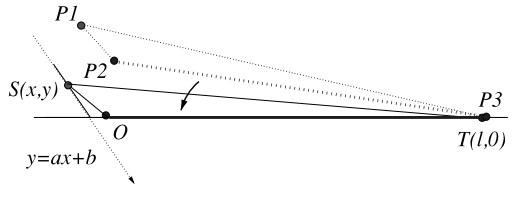

Fig. A·1 Monotone decrease in p.

$$+\sqrt{\left(\frac{2q(2q-1)}{r(4q-1)}-\frac{q}{r(4q-1)}\right)^2+\left(-\frac{2q-1}{r(4q-1)}-\frac{2q-1}{r(4q-1)}\right)^2}$$
$$-\sqrt{\left(\frac{2q(2q-1)}{r(4q-1)}+\frac{p}{r(4p-1)}\right)^2+\left(-\frac{2q-1}{r(4q-1)}-\frac{2p}{r(4p-1)}\right)^2}$$

and substitute 1 for p:

$$=\sqrt{\left(\frac{q}{r(4q-1)}+\frac{1}{3r}\right)^2+\left(\frac{2q-1}{r(4q-1)}-\frac{2}{3r}\right)^2}$$
$$+\sqrt{\left(\frac{2q(2q-1)}{r(4q-1)}-\frac{q}{r(4q-1)}\right)^2+\left(\frac{2(2q-1)}{r(4q-1)}\right)^2}$$
$$-\sqrt{\left(\frac{2q(2q-1)}{r(4q-1)}+\frac{1}{3r}\right)^2+\left(\frac{2q-1}{r(4q-1)}+\frac{2}{3r}\right)^2}$$
$$=\frac{1}{3r(4q-1)}\sqrt{(7q-1)^2+(-2q-1)^2}$$
$$+\frac{1}{r(4q-1)}\sqrt{16q^4-24q^3+9q^2+4(4q^2-4q+1)}$$
$$-\frac{1}{3r(4q-1)}\sqrt{(12q^2-6q+4q-1)^2+(14q-5)^2}$$
$$=\frac{1}{3r(4q-1)}\left(\sqrt{53q^2-10q+2}\right.$$
$$+3\sqrt{16q^4-24q^3+25q^2-16q+4}$$
$$\left.-\sqrt{144q^4-48q^3+172q^2-132q+26}\right).$$

Every term is bounded.
The first term:

$$\sqrt{53q^2-10q+2}\leqq\sqrt{53}q\quad\text{if}\quad\frac{1}{5}\leqq q.$$

The second term:

$$\sqrt{16q^4-24q^3+25q^2-16q+4}\leqq 4q^2-3q+2$$
$$\text{if } 0\leqq q.$$

The third term:

$$-\sqrt{144q^4-48q^3+172q^2-132q+26}$$
$$\leqq -(12q^2-2q).$$

Thus, we have

$$d(1,q)\leqq\frac{\sqrt{53}q+3(4q^2-3q+2)-(12q^2-2q)}{3r(4q-1)}$$
$$=\frac{(\sqrt{53}-7)q+2}{3r(4q-1)}.$$

This increases monotonically about q. So, we have

$$d(1,q)\leqq\lim_{q\to\infty}\frac{(\sqrt{53}-7)q+2}{3r(4q-1)}\approx\frac{0.2801}{12r}$$
$$=\frac{0.02334}{r}.$$

□

Tetsuo Asano received the M.E. and Ph.D. degrees from Osaka University in 1974 and 1977, respectively. He joined Osaka Electro-Communication University in 1977 as a lecturer. He joined Japan Advanced Institute of Science and Technology in 1997 where he is now a full professor. He has been working in computational geometry and VLSI design from theory to applications. He is serving as an editor for several journals including Discrete and Computational Geometry, Computational Geometry: Theory and Applications, International Journal of Computational Geometry and Applications, Theory of Computing Systems, etc. He is a Fellow of ACM and a member of SIAM, IPS of Japan, and Operations Research Society of Japan.

Yasuyuki Kawamura received the M.Sc. degree from Japan Advanced Institute of Science and Technology (JAIST) in 1999. He is a Ph.D. student in JAIST. He is interested in computational geometry, discrete mathematics and their applications.

Reinhard Klette is a professor of information technology in the department of computer science at the university of Auckland (New Zealand) and director of CITR Tamaki (Centre for Image Technology and Robotics). His research interests are directed on theoretical and applied subjects in image data computing, pattern recognition, image analysis, and image understanding. He has published journal and conference papers on different topics within computer science, and books about parallel processing, image processing, and shape recovery based on visual information.

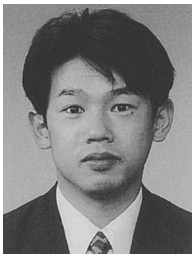

Koji Obokata received the B.E., M.E., and Ph.D. degrees from Gunma University in 1992, 1995, and 1998, respectively. Since 1998 he has been an associate in School of Information Science, Japan Advanced Institute of Science and Technology. He is interested in distributed algorithm, graph theory, computational geometry and their applications. He is a member of IPS of Japan.